JOURNAL OF SOLID STATE CHEMISTRY **128,** 289–294 (1997)
ARTICLE NO. SC967224

Structure and Properties of Zr_2Ni_2In and Zr_2Ni_2Sn

Rainer Pöttgen* and Richard Dronskowski†

*Anorganisch-Chemisches Institut, Universität Münster, Wilhelm-Klemm-Straße 8, D-48149 Münster, Germany; and
†Institut für Anorganische Chemie, RWTH Aachen, Professor-Pirlet-Straße 1, D-52056 Aachen, Germany

Received September 3, 1996; in revised form November 8, 1996; accepted November 12, 1996

Zr_2Ni_2In and Zr_2Ni_2Sn were prepared from the elements by a reaction in an arc melting furnace and subsequent annealing at 1070 K. They crystallize with the tetragonal Er_2Au_2Sn-type structure of space group $P4_2/mnm$, a ternary ordered version of the Zr_3Al_2-type. Both structures were refined from single-crystal X-ray data: $a = 715.1(1)$ pm, $c = 663.5(1)$ pm, $V = 0.3393(1)$ nm^3, $wR2 = 0.0442$, 324 F^2 values, 18 variables for Zr_2Ni_2In and $a = 703.2(1)$ pm, $c = 680.1(1)$ pm, $V = 0.3363(1)$ nm^3, $wR2 = 0.0668$, 240 F^2 values, 18 variables for Zr_2Ni_2Sn. The structures may be described as an intergrowth of *CsCl* and AlB_2 slabs. According to electronic structure calculations, the occurrence of the superstructure is a second order effect and most likely due to packing reasons (size of the zirconium cation). Compact polycrystalline samples of Zr_2Ni_2In and Zr_2Ni_2Sn are Pauli paramagnetic and metallic conductors.

INTRODUCTION

Recently, Zaremba and co-workers (1) reported on some new intermetallic compounds with the Mo_2FeB_2-type structure (ordered U_3Si_2-type) in the ternary systems (Zr, Hf)–(Co, Ni, Cu)–In. Their single-crystal structure refinement for Zr_2Ni_2In, assuming the ordered U_3Si_2-type structure (*tP*10, space group $P4/mbm$), showed a considerably large displacement parameter component B_{33} for the nickel atoms ($B_{33}/B_{11} = 6.1$), while all other anisotropic displacement parameters were normal. This effect already indicated that the nickel atoms are most likely not situated on the mirror plane. We had observed a similar behavior for the gold atoms in Er_2Au_2Sn (2), and our structure determination revealed that the latter compound crystallizes with the ordered Zr_3Al_2 structure (*tP*20, space group $P4_2/mnm$), a superstructure of U_3Si_2. The redetermination of the Zr_2Ni_2In structure, reported herein, indeed shows that the nickel atoms are shifted away from the mirror plane, as is also observed for isotypic Zr_2Ni_2Sn. In addition, we determined the magnetic and electrical properties of these intermetallic compounds and examined their electronic structures.

EXPERIMENTAL

Starting materials for the preparation of Zr_2Ni_2In and Zr_2Ni_2Sn were zirconium foil (Johnson Matthey, 0.2 mm thick), nickel wire (Johnson Matthey, $\varnothing$ 0.38 mm), indium tear drops (Johnson Matthey), and tin granules (Merck), all with stated purities better than 99.9%. In a first step, small pieces of the zirconium foil were melted down to buttons in an arc furnace under an argon pressure of about 800 mbar. The argon was purified before over molecular sieves, titanium sponge (900 K) and an oxisorb catalyst (3). These buttons were then melted together with the other elements in the ideal 2:2:1 atomic ratio. The melted ingots were turned over and remelted three times to ensure homogeneity. They were subsequently annealed in evacuated sealed silica tubes at 1070 K for 2 weeks.

Modified Guinier powder patterns (4) of all samples were recorded with Cu$K\alpha_1$ radiation using 5 *N* silicon ($a = 543.07$ pm) as an internal standard. The indexing of the diffraction lines was facilitated by intensity calculations (5) using the positional parameters of the refined structures. The lattice constants (Table 1) were obtained by least-squares refinements of the Guinier powder data. For Zr_2Ni_2In we observed good agreement with the data of Zaremba *et al.* (1), namely $a = 717.3(2)$ pm and $2c = 667.6(2)$ pm.

Single-crystal intensity data of Zr_2Ni_2In were collected on a four-circle diffractometer (Enraf-Nonius CAD4) with graphite monochromatized Ag$K\alpha$ radiation and a scintillation counter with pulse height discrimination. The intensity data for Zr_2Ni_2Sn were measured on a Stoe image plate system with graphite monochromatized Mo$K\alpha$ radiation with a detector distance of 50 mm and a constant counting time of 10 min per plate. The latter data were collected in the phi range from 0° to 180° with a phi step of 1°. All relevant data concerning the data collections are listed in Table 1.

The magnetic susceptibilities of polycrystalline pieces were determined with a SQUID magnetometer (Quantum Design, Inc.) between 4.2 and 300 K with a magnetic flux density of 1 T.

0022-4596/97 $25.00

TABLE 1
Crystal Data and Structure Refinement for Zr_2Ni_2In and Zr_2Ni_2Sn

Empirical formula	Zr_2Ni_2In	Zr_2Ni_2Sn
Formula weight	414.68 g/mol	418.55 g/mol
Temperature	293(2) K	293(2) K
Wavelength	56.086 pm	71.073 pm
Crystal system	tetragonal	tetragonal
Space group	$P4_2/mnm$ (No. 136)	$P4_2/mnm$ (No. 136)
Unit cell dimensions	$a = 715.1(1)$ pm	$a = 703.2(1)$ pm
(Guinier powder data)	$c = 663.5(1)$ pm	$c = 680.1(1)$ pm
	$V = 0.3393(1)$ nm^3	$V = 0.3363(1)$ nm^3
Formula units per cell	$Z = 4$	$Z = 4$
Calculated density	8.12 g/cm^3	8.28 g/cm^3
Crystal size	$50 \times 50 \times 75$ μm	$20 \times 45 \times 60$ μm
Data collection method	Enraf-Nonius, CAD4	Stoe image plate system
Absorption correction	from ψ-scan data	none
Transmission ratio (max/min)	0.945 : 0.623	n.a.
Absorption coefficient	29.08 mm^{-1}	24.01 mm^{-1}
$F(000)$	740	744
θ range for data collection	2° to 24°	6° to 28°
Range in hkl	$+8, +10, \pm 9$	$\pm 10, \pm 9, \pm 9$
Total no. reflections	1008	2699
Independent reflections	325 ($R_{int} = 0.0273$)	241 ($R_{int} = 0.0911$)
Reflections with $I > 2\sigma(I)$	267 ($R_{sigma} = 0.0226$)	225 ($R_{sigma} = 0.0350$)
Refinement method	Full-matrix least-squares on F^2	Full-matrix least-squares on F^2
Data/restraints/parameters	324/0/18	240/0/18
Goodness-of-fit on F^2	1.179	1.146
Final R indices $[I > 2\sigma(I)]$	$R1 = 0.0201$, $wR2 = 0.0396$	$R1 = 0.0276$, $wR2 = 0.0645$
R indices (all data)	$R1 = 0.0330$, $wR2 = 0.0442$	$R1 = 0.0298$, $wR2 = 0.0668$
Extinction coefficient	0.0031(5)	0.007(1)
Largest diff. peak and hole	943 and -874 e/nm^3	2544 and -1812 e/nm^3

The specific resistivities were measured on small blocks ($1.4 \times 1.2 \times 1.6$ mm^3 for Zr_2Ni_2In and $2.8 \times 2.8 \times 1.0$ mm^3 for Zr_2Ni_2Sn) with a conventional four-probe technique. Cooling and heating curves measured between 4.2 and 300 K were identical within error bars, also for different samples.

Three-dimensional band structure calculations were based on an extended Hückel Hamiltonian (6, 7), whereas off-site Hamiltonian matrix elements were evaluated according to the weighted Wolfsberg–Helmholz formula (8), minimizing counterintuitive orbital mixing. The minimal orbital basis set was composed of Slater orbitals that had been scaled to j-averaged values of numerical Dirac–Fock atomic functions; on-site Hamiltonian matrix elements were approximated by averaged atomic orbital energies from the same source (9, 10). To obtain greater accuracy, the Zr 4d and Ni 3d atomic wave functions were approximated by double zeta functions. All exchange integrals, ξ orbital exponents, and weighting coefficients are listed in Table 2. The eigenvalue problem was solved in reciprocal space at 90 k points within the irreducible wedge of the Brillouin zone by using a modified EHMACC code (11).

TABLE 2
Extended Hückel Parameters

Atom	Orbital	H_{ii} (eV)	ξ_1 (c_1)	ξ_2 (c_2)
Zr	5s	-5.86	1.366	
	5p	-3.68	0.987	
	4d	-7.93	2.769 (0.650)	1.224 (0.508)
Ni	4s	-7.66	1.535	
	4p	-4.29	1.010	
	3d	-18.52	6.339 (0.486)	2.625 (0.658)
In	5s	-10.79	2.023	
	5p	-5.35	1.367	
Sn	5s	-13.88	2.224	
	5p	-6.79	1.620	

RESULTS AND DISCUSSION

Powders and single crystals of Zr_2Ni_2In and Zr_2Ni_2Sn are light grey and stable in air over long periods of time. No decomposition whatsoever was observed after several months. Single crystals exhibit metallic luster. They have very irregular platelet-like shape.

Lattice Constants

The structural similarity of Zr_2Ni_2In and Zr_2Ni_2Sn with the ordered U_3Si_2-type structure was instantly visible from the modified Guinier powder patterns (4), however, on both patterns additional weak reflections remained. Both patterns could only be completely indexed upon doubling the tetragonal unit cell along c indicating that both compounds adopt the ordered Zr_3Al_2 structure, a superstructure of U_3Si_2. The strongest superstructure reflections (with relative intensities in parentheses) for Zr_2Ni_2Sn occurred between $2\theta = 19°$ and 22°: 221 (1.8%), 103 (3.1%), 311 (1.9%), and 113 (1.5%). The same result was also obtained for Er_2Au_2Sn (2), Ti_2Ni_2In, and Zr_2Pd_2In (12). These compounds also crystallize with the ordered Zr_3Al_2-type.

Structure Refinements

Single crystals of Zr_2Ni_2In and Zr_2Ni_2Sn were isolated from the crushed samples after the annealing process and then examined by Buerger precession photographs to establish both symmetry and suitability for intensity data collection. The photographs showed tetragonal Laue symmetry

4/*mmm* and the before mentioned doubling of the cell along *c*. The systematic extinctions (0*kl* observed only with $k + l = 2n$, *h*00 only with $h = 2n$) led to the space groups $P4_2/mnm$, $P\bar{4}n2$, and $P4_2nm$, of which the centrosymmetric group $P4_2/mnm$ (No. 136) was found to be correct, in agreement with the previous investigation on Er_2Au_2Sn (2). All relevant crystallographic data and experimental details are listed in Table 1.

The atomic positions of Er_2Au_2Sn (2) were taken as starting values and both structures were successfully refined using SHELXL-93 (13), with anisotropic displacement parameters for all atoms. Within each refinement, one reflection with $F_o^2 < -2\sigma(F_o^2)$ was treated as unobserved (13). Final difference Fourier syntheses were flat and revealed no significant residual peaks. The results of the refinements are summarized in Table 1. Atomic coordinates and interatomic distances are listed in Tables 3 and 4. Listings of the anisotropic displacement parameters and the observed and calculated structure factors are available.[1]

TABLE 3
Atomic Coordinates and Isotropic Displacement Parameters (pm^2) for Zr_2Ni_2In and Zr_2Ni_2Sn

Atom	Wyckoff site	*x*	*y*	*z*	U_{eq}[a]
		Zr_2Ni_2In			
Zr1	4*f*	0.17470(6)	*x*	0	56(2)
Zr2	4*g*	0.33832(6)	$-x$	0	58(2)
Ni	8*j*	0.37454(8)	*x*	0.26648(9)	73(2)
In	4*d*	0	1/2	1/4	63(2)
		Zr_2Ni_2Sn			
Zr1	4*f*	0.18305(10)	*x*	0	70(3)
Zr2	4*g*	0.34462(10)	$-x$	0	74(3)
Ni	8*j*	0.37400(10)	*x*	0.28410(14)	82(3)
Sn	4*d*	0	1/2	1/4	79(3)

[a] U_{eq} is defined as one third of the trace of the orthogonalized U_{ij} tensor.

Crystal Chemistry

Our structure refinements of Zr_2Ni_2In and Zr_2Ni_2Sn show that both compounds adopt the Er_2Au_2Sn (2) structure, a ternary ordered version of Zr_3Al_2, which itself may be considered as a superstructure of U_3Si_2. The Zr_3Al_2 and U_3Si_2 structure, and thus also the ternary ordered versions, are crystallographically related by a group–subgroup scheme: $P4_2/mnm$ (Zr_3Al_2) is a *klassengleich* subgroup (index 2) of *P*4/*mbm* (14). A more detailed description of the structural relationships was already given in Ref. (12).

A projection of the Zr_2Ni_2Sn structure is shown in Fig. 1. The structure is built up from distorted AlB_2- and CsCl-like fragments of compositions *ZrNi*$_2$ and *ZrSn* outlined in this figure. Due to the strong distortions, both the AlB_2 and CsCl slab have lost their hexagonal and cubic symmetry, respectively. In the superstructure, the nickel atoms have moved away from the mirror planes perpendicular to *z* by 10.9(1) pm in Zr_2Ni_2In and by 23.2(1) pm in Zr_2Ni_2Sn. A cutout of the *ZrNi*$_2$ fragment is presented in Fig. 2. The breathing of the zirconium prisms is pronounced in Zr_2Ni_2Sn. The prism ground plane contracts if two Ni_2 pairs move away from it, while the planes above and below expand. The displacement of the Ni_2 pairs in Zr_2Ni_2Sn results in shorter (293.7 pm) and longer (386.4 pm) Ni–Ni distances along *c*. The Ni–Ni distance within the Ni_2 pair of 250.6 pm is close to the Ni–Ni bond length of 249.2 pm in fcc nickel (15). On the other hand, the zirconium atoms remain on the mirror planes but move along the *xy* diagonal (see Fig. 1). While both of these distortions are only small in Zr_2Ni_2In, they are stronger in Zr_2Ni_2Sn. The nickel atoms in the stannide show the largest displacement from the mirror planes among the compounds with the ordered Zr_3Al_2 structure (2, 12, 16).

TABLE 4
Interatomic Distances (pm) in Zr_2Ni_2In and Zr_2Ni_2Sn

Zr_2Ni_2In				Zr_2Ni_2Sn			
Zr1:	4	Ni	267.1	Zr1:	4	Ni	265.3
	2	Ni	268.5		2	Ni	270.9
	4	In	311.8		4	Sn	308.5
	2	Zr2	332.0		2	Zr2	341.2
	1	Zr1	353.3		2	Zr2	351.0
	2	Zr2	367.4		1	Zr1	364.1
	2	Zr2	385.1		2	Zr2	388.1
Zr2:	2	Ni	265.2	Zr2:	2	Ni	262.4
	4	Ni	272.2		4	Ni	277.3
	4	In	315.3		1	Zr2	309.0
	1	Zr2	327.0		4	Sn	315.6
	2	Zr1	332.0		2	Zr1	341.2
	2	Zr1	367.4		2	Zr1	351.0
	2	Zr1	385.1		2	Zr1	388.1
Ni:	1	Ni	253.8	Ni:	1	Ni	250.6
	1	Zr2	265.2		1	Zr2	262.4
	2	Zr1	267.1		2	Zr1	265.3
	1	Zr1	268.5		1	Zr1	270.9
	2	Zr2	272.2		2	Zr2	277.3
	2	In	282.7		2	Sn	278.5
	1	Ni	309.9		1	Ni	293.7
In:	4	Ni	282.7	Sn:	4	Ni	278.5
	4	Zr1	311.8		4	Zr1	308.5
	4	Zr2	315.3		4	Zr2	315.6
	2	In	331.8		2	Sn	340.1

Note. All distances shorter than 475 pm (Zr–Zr, Zr–Ni, Zr–In, Zr–Sn, In–In, Sn–Sn), 420 pm (Ni–In, Ni–Sn), and 350 pm (Ni–Ni) are listed. Standard deviations are all equal or less than 0.1 pm.

[1] Details may be obtained from: Fachinformationszentrum Karlsruhe, D-76344 Eggenstein-Leopoldshafen (Germany), by quoting the registry numbers CSD-405563 (Zr_2Ni_2In) and CSD-405564 (Zr_2Ni_2Sn).

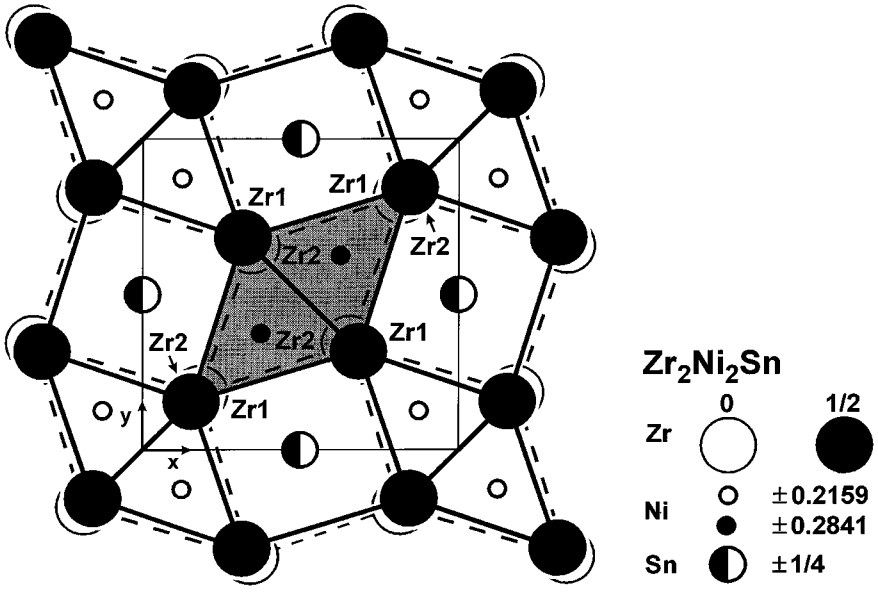

FIG. 1. Projection of the crystal structure of Zr_2Ni_2Sn along the *c* axis. The distorted AlB_2- and CsCl-related fragments are emphasized. The shaded trigonal prisms correspond to the cutout presented in Fig. 2.

In comparison, it is interesting to note that the $[Ni_2Sn]$ polyanion in Zr_2Ni_2Sn (Fig. 3) has a coordination very similar to the binary phosphide PdP_2 (17). In Zr_2Ni_2Sn, the $[Ni_2Sn]$ polyanions are slightly puckered (nickel dislocation) and separated by the zirconium atoms. The PdP_2

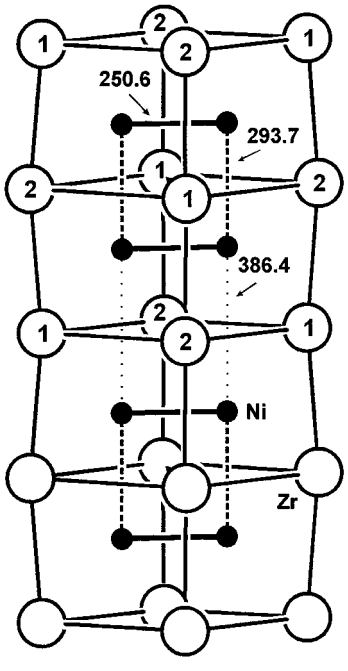

FIG. 2. Cutout of the Zr_2Ni_2Sn structure: A row of trigonal prisms consisting of four distorted AlB_2 slabs of composition $ZrNi_2$ is shown together with some relevant interatomic distances.

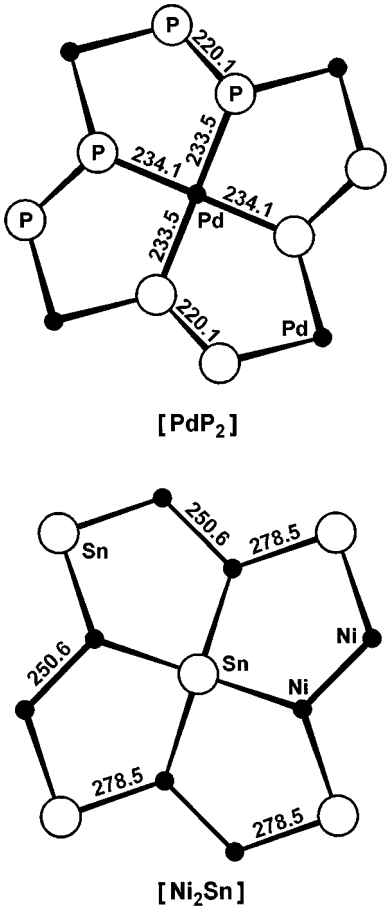

FIG. 3. Cutouts of the PdP_2 structure and of the $[Ni_2Sn]$ polyanion of Zr_2Ni_2Sn. Relevant interatomic distances and atom designations are given.

layers in the binary phosphide are also puckered and directly connected to each other via P–P bonds, with the phosphorus atoms forming one-dimensional infinite zigzag chains. The structural similarity is also paralleled by a similar polarity within the PdP_2 and $[Ni_2Sn]$ layers. According to the (8-N) rule, PdP_2 may be described as a zintl phase with the formula $Pd^{2+}(^1_\infty P^-)_2$. In the $[Ni_2Sn]$ polyanions, the nickel pairs carry a negative charge (see below), while a positive charge is found for the tin atoms.

Electronic Structure

It seems convenient to compare the results of the band structure calculations with those recently obtained (18) for the intermetallic compound Sc_2Ni_2In, crystallizing in the simple, ordered U_3Si_2 structure without cell doubling along *c*. Sc_2Ni_2In is a nickelide, with electron density flowing from indium to nickel while the scandium atoms remain almost neutral.

In contrast, the gross Mulliken charges for Zr_2Ni_2In ($Zr_{(average)}$: + 0.51, Ni: − 0.97, In: + 0.92) and Zr_2Ni_2Sn ($Zr_{(average)}$: + 0.54, Ni: − 0.97, Sn: + 0.86) reveal a significantly higher charge for zirconium (compared to scandium) and, consequently, a reduced charge for the main group element. Surprisingly, this course is counterintuitive to the absolute electronegativities of scandium and zirconium (19). The charge difference between the two Zr1 and Zr2 positions is smaller than 25% in both compounds, with the Zr1 position being higher charged because of having the closer contacts to electronegative nickel.

We have tried to determine the reason for the formation of the superstructure by performing total energy calculations for both compounds, considering first the real crystal structure and then the averaged (subcell) structure. As it turns out, the electronic structure calculations do indeed (accidentally?) favor the experimentally found superstructure with respect to the subcell structure, however, the energy differences are extraordinarily small, namely 8 kJ/mol for Zr_2Ni_2Sn (23 pm nickel dislocation from the subcell mirror plane) and 2 kJ/mol for Zr_2Ni_2In (11 pm dislocation). While such tiny differences can surely not be counted on (considering the limited accuracy of the method used), it is nevertheless clear that any *simple*, molecular-orbital-like explanation for the superstructure, i.e., occupation of a particular one-electron band, may be ruled out. For comparison, Fig. 4 offers two theoretical densities-of-states (DOS) for the case of Zr_2Ni_2Sn, being almost indistinguishable for the naked eye. There is a *slightly* reduced, zirconium centered DOS at the Fermi level only for the real superstructure.

Related molecular orbital model calculations for a cluster containing 16 zirconium and 6 nickel atoms (3 $ZrNi_2$ slabs stacked as in Fig. 2), either naked or saturated with an additional hydrogen atom surface, did not show any significant nickel contribution to the valence levels such that an electronic origin for the observed nickel dislocations is unlikely. On the contrary, one may think of the Ni_2 pair movement along *z* as being a second-order effect, reflecting the zirconium substructure breathing (short Zr2–Zr2 and long Zr1–Zr1 distances) which results from mainly Zr–Zr δ interactions around − 8.2 eV. The latter bonding optimization slightly reduces the DOS at the Fermi level (see above).

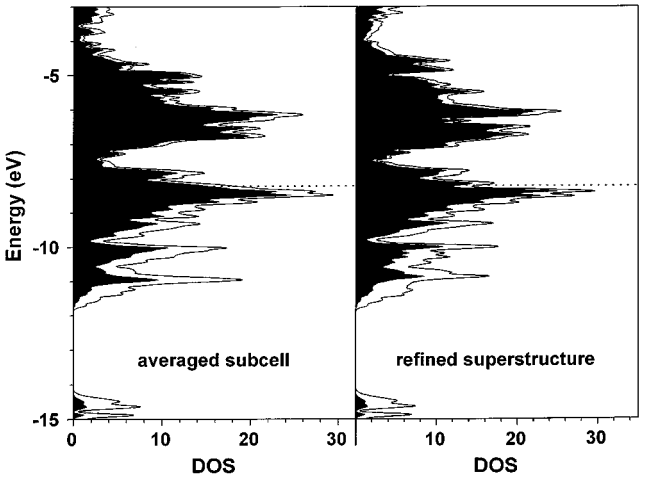

FIG. 4. Density-of-states (DOS) of Zr_2Ni_2Sn with the zirconium contributions emphasized in black. The left-hand DOS corresponds to the average structure (subcell) of Zr_2Ni_2Sn, whereas the right-hand DOS corresponds to the refined X-ray structure (superstructure).

Moreover, a systematic comparison (20) of the compounds R_2Au_2In (R = Y, Gd–Tm, Lu) suggests a geometric explanation for these specific distortions in the zirconium substructure. Only Tm_2Au_2In and Lu_2Au_2In, containing the smallest rare earth atoms, adopt the superstructure, while all those with larger rare earth atoms do not. We thus propose that the effective size of the zirconium atom in Zr_2Ni_2Sn and Zr_2Ni_2In is smaller than the one of scandium in Sc_2Ni_2In, a direct consequence of the higher cationic charge of zirconium compared to scandium (see above).

Magnetic and Electrical Properties

The temperature dependences of the magnetic susceptibility of Zr_2Ni_2Sn and Zr_2Ni_2In are shown in Fig. 5. Above about 50 K the susceptibilities do not significantly vary with temperature, indicating Pauli paramagnetism. The room temperature susceptibilities amount to $2.7(1)\times10^{-4}$ emu/mol for Zr_2Ni_2In and $2.3(1)\times10^{-4}$ emu/mol for Zr_2Ni_2Sn. This compares well with the room temperature susceptibility of $3.8(1)\times10^{-4}$ emu/mol of Sc_2Ni_2In (18). At low temperatures both suceptibilities increase, most likely due to very small amounts of paramagnetic impurities, although

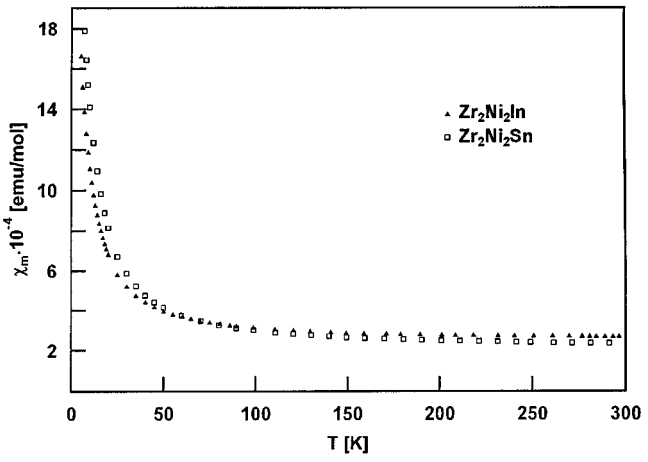

FIG. 5. Temperature dependence of the magnetic susceptibilities of Zr_2Ni_2In and Zr_2Ni_2Sn measured at a magnetic flux density of 1 T.

the Guinier powder patterns showed single phase samples. A similar temperature dependence was recently also observed for Ti_2Ni_2In, Zr_2Co_2In, and Zr_2Pd_2In (12).

The specific resistivities of Zr_2Ni_2In and Zr_2Ni_2Sn decrease with decreasing temperature (Fig. 6), as is typical for metals. The room temperature value of the specific resistivity amounts to 280 μΩ cm for both compounds. Thus, Zr_2Ni_2In and Zr_2Ni_2Sn are good metallic conductors when compared to the specific resistivities of 6.84 and 8.37 μΩ cm for nickel and indium at room temperature, respectively (21).

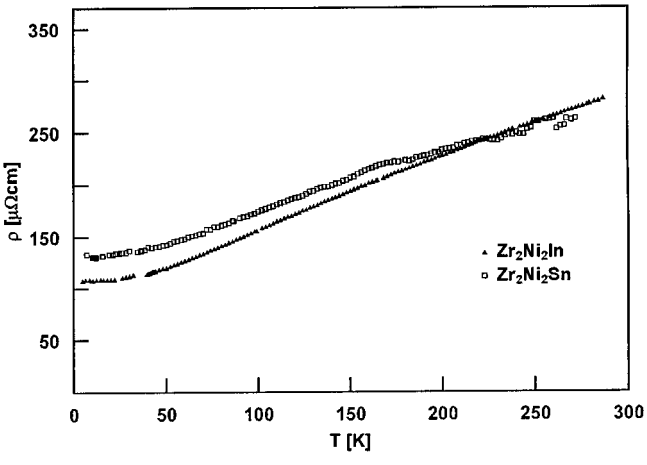

FIG. 6. Temperature dependence of the specific resistivities of Zr_2Ni_2In and Zr_2Ni_2Sn.

ACKNOWLEDGMENTS

We thank Professor Arndt Simon and Professor Wolfgang Jeitschko for their interest and steady support of this work. We are also grateful to Willi Röthenbach for taking the Guinier powder patterns, to Eva Brücher and Dr. Reinhard K. Kremer for the susceptibility measurements, and to Nicola Rollbühler for the electrical conductivity measurement. This work was supported by the Deutsche Forschungsgemeinschaft and the Fonds der Chemischen Industrie.

REFERENCES

1. V. I. Zaremba, L. D. Gulai, Ya. M. Kalychak, and L. G. Aksel'rud, *Crystallogr. Rep.* **40,** 334 (1995).
2. R. Pöttgen, *Z. Naturforsch. B* **49,** 1309 (1994).
3. H. L. Krauss and H. Stach, *Z. Anorg. Allg. Chem.* **366,** 34 (1969).
4. A. Simon, *J. Appl. Crystallogr.* **4,** 138 (1971).
5. K. Yvon, W. Jeitschko, and E. Parthé, *J. Appl. Crystallogr.* **10,** 73 (1977).
6. R. Hoffmann, *J. Chem. Phys.* **39,** 1397 (1963).
7. Roald Hoffmann, "Solids and Surfaces: A Chemist's View of Bonding in Extended Structures." VCH, Weinheim, New York, 1988.
8. J. H. Ammetter, H.-B. Bürgi, J. C. Thibeault, and R. Hoffmann, *J. Am. Chem. Soc.* **100,** 3686 (1978).
9. J. P. Desclaux, *At. Data Nucl. Data Tables* **12,** 3110 (1973).
10. P. Pyykkö and L. L. Lohr, Jr., *Inorg. Chem.* **20,** 1950 (1981).
11. M. H. Whangbo, M. Evain, T. Hughbanks, M. Kertesz, S. Wijeyesekera, C. Wilker, C. Zheng, and R. Hoffmann, "QPCE program EHMACC."
12. R. Pöttgen and G. Kotzyba, *Z. Naturforsch. B* **51,** 1248 (1996).
13. G. M. Sheldrick, "SHELXL-93, Program for Crystal Structure Refinement," University of Göttingen, Germany, 1993.
14. H. Bärnighausen, *Commun. Math. Chem.* **9,** 139 (1980).
15. J. Donohue, "The Structures of the Elements," Wiley, New York, 1974.
16. P. Gravereau, F. Mirambet, B. Chevalier, F. Weill, L. Fournès, D. Laffargue, F. Bourée, and J. Etourneau, *J. Mater. Chem.* **4,** 1893 (1994).
17. W. H. Zachariasen, *Acta Crystallogr.* **16,** 1253 (1963).
18. R. Pöttgen and R. Dronskowski, *Z. Anorg. Allg. Chem.* **622,** 355 (1996).
19. R. G. Pearson, *Inorg. Chem.* **27,** 734 (1988).
20. R. Pöttgen, *Z. Naturforsch. B* **49,** 1525 (1994).
21. R. C. Weast (Ed.), "Handbook of Chemistry and Physics," 59th ed., CRC Press, Boca Raton, 1978.